Freestanding Positionable Microwave-Antenna Device for Magneto-Optical **Spectroscopy Experiments**

T. Hache, 1,2,* M. Vaňatka, L. Flajšman, T. Weinhold, 1,4 T. Hula, 1,2 O. Ciubotariu, M. Albrecht, 5 B. Arkook, ⁶ I. Barsukov⁰, ⁶ L. Fallarino, ¹ O. Hellwig, ^{1,2} J. Fassbender, ^{1,4} M. Urbánek⁰, ³ and H. Schultheiss 1,4

¹Helmholtz-Zentrum Dresden–Rossendorf, Institute of Ion Beam Physics and Materials Research, Bautzner Landstraße 400, 01328 Dresden, Germany ²Institut für Physik, Technische Universität Chemnitz, 09107 Chemnitz, Germany ³ CEITEC BUT, Brno University of Technology, Purkyňova 123, 612 00 Brno, Czech Republic ⁴ Technische Universität Dresden, 01062 Dresden, Germany ⁵ Institute of Physics, University of Augsburg, Universitätsstraße 1, 86135 Augsburg, Germany ⁶Physics and Astronomy, University of California, Riverside, California 92521, USA

(Received 3 December 2019; revised manuscript received 6 March 2020; accepted 8 April 2020; published 5 May 2020)

Modern spectroscopic techniques for the investigation of magnetization dynamics in micro and nanostructures or thin films typically use microwave antennas. They are directly fabricated on top of the sample by means of electron-beam lithography (EBL). Following this approach, every magnetic structure on the sample needs its own antenna, resulting in additional EBL steps and layer-deposition processes. Here, we demonstrate an approach for magnetization excitation that is suitable for optical and nonoptical spectroscopy techniques. By patterning the antenna on a separate flexible glass cantilever and insulating it electrically, we solve the mentioned issues. Since we use flexible transparent glass as the antenna substrate, optical spectroscopy techniques like microfocused Brillouin-light-scattering microscopy (μ BLS), time-resolved magneto-optical Kerr-effect measurements, or optically detected magnetic resonance measurements can be carried out at visible laser wavelengths. As the antenna is detached from the sample it can be freely positioned in all three dimensions to address only the desired magnetic structures and to achieve an effective excitation. We demonstrate the functionality of these antennas using μ BLS and compare coherently and thermally excited magnon spectra to reveal an enhancement of the signal by a factor of about 400 due to the strong excitation by the antenna. Moreover, we succeed in characterizing yttrium-iron-garnet thin films with spatial resolution using optical ferromagnetic resonance experiments. We analyze the spatial excitation profile of the antenna by measuring the magnetization dynamics in two dimensions. The technique is furthermore applied to investigate injection locking of spin Hall nano-oscillators in the most favourable geometry with the highest spin-torque efficiency.

DOI: 10.1103/PhysRevApplied.13.054009

I. INTRODUCTION

The investigation of magnetization dynamics for research on computational techniques that could allow for faster data processing with higher-energy efficiency is of considerable general interest. Magnonics and spintronics are promising fields in order to achieve this revolution in data processing by using spin-wave-based computing [1,2]. However, for these new techniques more fundamental and material research needs to be performed. In particular, alternative materials with low damping for improved spin-wave propagation or enhanced nonlinear effects at moderate pump powers as well as excitation methods are needed.

In order to compete with today's computational schemes, new techniques need to operate on the nanoscale and make the use of thin-film technology necessary. Therefore, new materials are mostly deposited as thin films first, which allows for characterization by standard techniques like ferromagnetic resonance (FMR), magnetooptical Kerr-effect measurements (MOKE) [3], and vibrating sample magnetometry (VSM) [4].

On the other hand, to investigate spin-wave propagation in materials and microstructures other techniques have to be used. Spin waves can be measured electrically by propagating spin-wave spectroscopy [5–7] using antennas with a defined wave-vector (k) excitation but

^{*}t.hache@hzdr.de

without spatial resolution of the spin-wave propagation. Another promising technique is Brillouin-light-scattering microscopy (µBLS) [8], which is able to detect coherently excited spin waves as well as incoherent thermal spin waves spatially and time resolved. This technique is based on the inelastic scattering of light by spin waves, which leads to a frequency shift of the scattered laser light. Moreover, the spin-wave dispersion relation can be investigated by phase-resolved measurements. Due to these features our method has significant advantages compared to the nearfield microwave spectroscopy microscopy [9–11], which uses conductive loops to probe the magnetization dynamics spatially resolved. While for this technique the spatial resolution is limited to the loop diameter, our technique has an enhanced resolution, since the limit is given by the laser-spot diameter of about 320 nm. Furthermore, propagating spin waves can be investigated up to a wave vector of about 17 rad/ μ m. In contrast to other optical, spatial, and time-resolved techniques using separated pump and probe beams [12–15], where the magnetization is excited by a broad frequency spectrum provided by the laser pulse, in our case the frequency is clearly defined by the microwave source. Regardless of whether electrical or optical techniques are used, up to now antennas for the excitation of the spin waves need to be patterned on the sample. This is a rather complex, time, and resourceconsuming process. Moreover, on conductive substrates (e.g., epitaxial iron grown on single-crystal copper) [16] with a required insulating layer below the antenna, contacting with probes can destroy this insulation. Here, we demonstrate an alternative approach. We separate the antenna used for excitation of the magnetization from the sample. This makes the antenna freely positionable with respect to the sample under investigation and allows for probing the spin-wave dynamics locally, whereas standard FMR measurements integrate over a large area [17–19]. Furthermore, the relative orientation between the antenna and the magnetic element can be easily varied. This allows spin waves to be probed in the same magnetic microstructure for different angles of the applied magnetic field. Since the antenna can be easily removed in contrast to antennas that are patterned directly on the sample, different dynamic field configurations can be applied. The possibility of reusing the antennas offers the additional advantage that these single antennas need to be characterized only once regarding their frequency-dependent transmission function.

II. SPECIFICATIONS OF THE ANTENNA DEVICE

Figure 1(a) shows schematically the suspended antenna in operation (not to scale) measuring micrometer-sized magnetic elements exemplarily. It is separated from the sample under investigation and patterned on a glass substrate, which is held by an adapter unit. It is fixed on

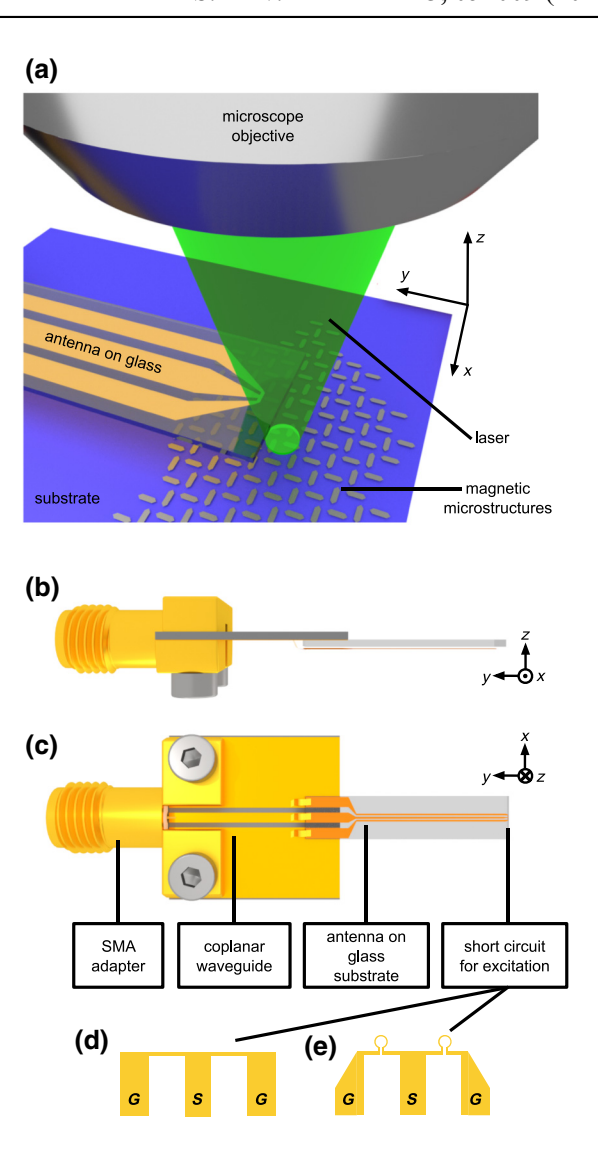


FIG. 1. (a) Measurement scheme (not to scale, x and y direction in the sample plane). The suspended antenna providing local excitation of magnetic elements is fabricated on a glass cantilever allowing light transmission for magneto-optical experiments like BLS. The sample and the antenna device can be moved independently from each other. (b) Side view. (c) An SMA adapter connects the suspended antenna to external microwave equipment. The suspended antenna is fabricated on a $100-\mu m$ -thick glass substrate, which is bonded and fixed on a coplanar waveguide connected to the SMA adapter. A current through the short circuits between ground (G) and signal (S) lines generates a dynamic magnetic Oersted field, which can be used to excite the magnetization. (d) Straight-line short circuit. (e) Omega-loop short circuit for effective out-of-plane excitation.

a micrometer manipulator and can be moved along all three axes in order to reach every measurement position on the sample, which is given by the focused laser spot in magneto-optical experiments like μ BLS. The free-standing antenna and the sample are held together on an additional x-y-z stage, which allows both to be moved

below the laser spot. By driving this stage sequentially between the focus points on the sample and the antenna, the distance between both can be measured with submicrometer accuracy. Figures 1(b) and 1(c) present the actual device in side view and top view, respectively. A subminiature A (SMA) adapter at the bottom is used to connect the suspended antenna to signal generators by standard SMA cables. This adapter is soldered to a coplanar waveguide fabricated on a high-frequency printed circuit board (PCB). On this PCB the glass substrate is fixed and wirebonded using $20 \times 250 \ \mu\text{m}^2$ ribbons. It is the actual part carrying the antenna structure, which is patterned by electronbeam lithography (EBL). The conductive layer as well as an additional SiO₂ insulating layer are deposited by electron-beam evaporation. This insulating layer protects the antenna's coplanar waveguide from being shorted by a conductive sample if they are in contact. The signal and both ground lines are short circuited at the end in order to allow a current flow generating a dynamic magnetic Oersted field that excites the magnetization in the sample. The shape of the short circuit can be adjusted regarding the experimental needs for example straight line wires as shown in Fig. 1(d) for in-plane, or in Fig. 1(e), omegashaped loops for out-of-plane excitation, respectively. We measured the resistance of the antenna at various nominal microwave powers up to 30 dBm. We only find a little resistance increase of about 2%. Therefore, we conclude that antenna heating does not play a significant role in our experiments.

An important property of the antenna is the possibility to change the distance between sample and antenna. Figure 2(a) shows the calculated Oersted field for a current-carrying wire with a rectangular shape. The width is 1 μ m and the height 600 nm, corresponding to the actual dimensions of the used antenna short circuit. Since the skin depth of a microwave current in a frequency range up to 20 GHz is larger than the antenna dimensions, the field calculations can be approximated with static currents and a value of 63 mA is chosen. It corresponds to a microwave power of 20 dBm assuming that the wire is a 50-Ohm termination of a microwave waveguide. If the sample is in direct contact with the antenna, the magnetic field interacting with the sample is extracted along the red dashed line. The out-of-plane (z) and in-plane (y) component of this field are extracted and are shown in Figs. 2(b) and 2(c) as the 0-nm case, respectively. Moreover, the plots show the field distribution for a variable distance between antenna and sample from 0 to 60 μ m. By increasing the distance, the maximal field strength decreases, but its homogeneity increases. To investigate this effect further, we made a Fourier transform of the spatial distribution of the magnetic field in order to exctract information about spatial frequencies, which are plotted in Fig. 2(d). It can be clearly seen that the field amplitudes for small k vectors are significantly larger than for large k vectors. By increasing

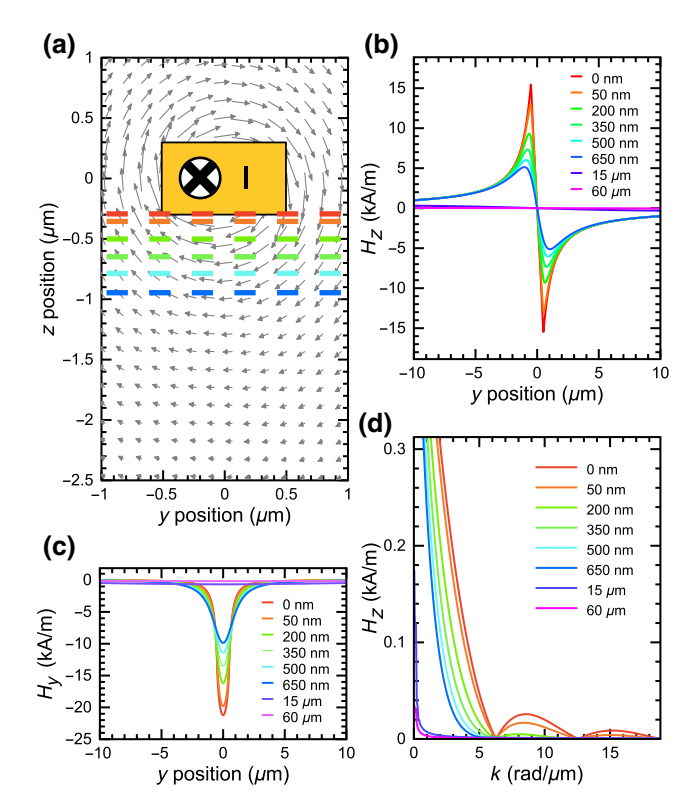


FIG. 2. (a) Calculated Oersted field around the short circuit of the antenna with rectangular shape (parameters: width, 1 μ m; height, 600 nm; dc current, 63 mA). The strength and local orientation of the field are denoted by the arrows. The dashed lines indicate the z position, where the field distribution is analyzed. (b) z component of the Oersted field extracted along the dashed lines for different distances between antenna and sample. (c) y component of the Oersted field extracted along the dashed lines for different distances between antenna and sample. (d) Fourier transform of the field distributions shown in (b).

the distance between antenna and sample, the field amplitudes at higher \mathbf{k} values are even more suppressed. Only for larger distances the field amplitudes drop dramatically.

III. TIME-EFFICIENT CHARACTERIZATION OF MAGNETIC FILMS

The magneto-dynamic properties of newly developed materials can effectively be characterized by BLS in the case of sufficient cross section of the light with the material, which can therefore probe the dynamic magnetic modes. Usually, the new materials are deposited as thin films or even as nanoparticles on flat substrates. The typical approach for first tests is the measurement of the thermally excited, incoherent spin waves in these samples, which can, depending on the material, become a very time-consuming and rather inefficient task. In some materials, which are even transparent for the used laser light, these measurements can take hours or the obtained signals

are even hidden in the counting noise of the photo detector. In this section we demonstrate a much more efficient approach for the characterization of materials and the possibility of obtaining an estimate for material parameters by carrying out optical FMR measurements.

As a first proof of concept we show in Fig. 3 the direct comparison of the measured BLS counts of thermally excited spin waves in a Pt(4.5 nm)/Cu(0.87 nm)/Py(5 nm)/Al(3.5 nm) film with the strong signal when the antenna is used to excite the magnetization dynamics. An external in-plane field of 51 mT is applied and the antenna is connected to a signal generator outputting 6 GHz at a nominal power of 30 dBm. Notice that both measurements are performed through the glass cantilever in order to obtain comparable measurement conditions. The direct comparison shows an increase of the BLS counts by a factor of about 400 for the same measurement time. Additionally, we plot the peak intensity for different microwave excitations to demonstrate that dynamics can be driven over a wide frequency range. Even though the largest intensity is reached around the ferromagnetic resonance we observe a significant increase for higher frequencies up to 6.6 GHz, which corresponds to a wave vector of 7 rad/ μ m. This is a clear demonstration of the utility of our technique. Due to the enhanced magnon intensity the total number of accumulated BLS spectra can be reduced, which decreases measurement time. Notice that we use a sample that shows a sufficient thermal spectrum within several minutes in order to compare the BLS counts with and without antenna excitation. In addition, we calculate the spin-wave dispersion relation [20] for a 5-nm-thick Py thin film to compare

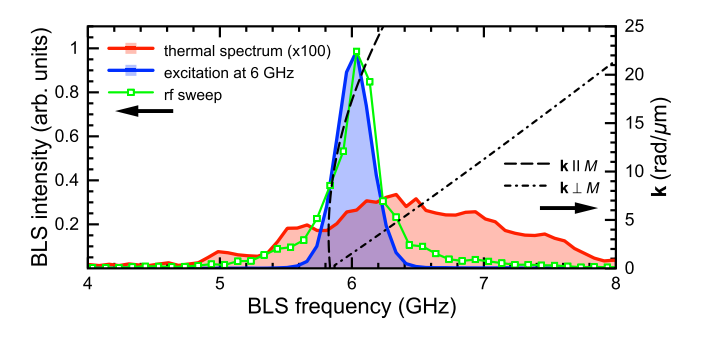


FIG. 3. Comparison of BLS spectra without (red) and with (blue) antenna excitation at 6 GHz and a nominal power of 30 dBm measured on a Pt(4.5 nm)/Cu(0.87 nm)/Py(5 nm)/Al(3.5 nm) film. A thermal spin-wave band can be measured between 5 and 8 GHz at $B_{\rm ex}=51$ mT. By applying a microwave current to the antenna the signal at the excitation frequency can be increased by a factor of about 400. The green curve shows the reached BLS intensity maxima during the rf excitation at the corresponding frequencies. The dashed and dash-dotted lines show the spin-wave band between propagating spin waves parallel or perpendicular to the magnetization direction for the used parameters: $M_S=640$ kA/m, $\gamma/2\pi=28$ GHz/T, and $A_{\rm ex}=10$ pJ/m.

it with the frequency range of the measured thermal spin-wave band and the frequency with the highest spin-wave amplification caused by the antenna. Regarding the calculations shown in Fig. 2 we expect an efficient coupling of the microwave field of the antenna to the magnetization close to the FMR mode. This can be verified since the highest amplification of the spin waves is found at 6 GHz. Please note that the reduction of spin-wave intensities above 7.5 GHz is due to experimental limitations. Here the used microscope objective lens limits the detection to $\bf k$ vectors below 17 rad/ μ m [8].

As a next step, we show an optical FMR measurement using BLS on a 50-nm-thick yttrium-iron-garnet (Y₃Fe₅O₁₂, YIG) film, which is grown epitaxially by pulsed laser deposition on a Gd₃Ga₅O₁₂(111) substrate. YIG is transparent for the used 532-nm laser and backscattering due to thermal spin waves has a very small cross section. However, by using the antenna for the excitation of the magnetization the measurement of ferromagnetic resonance curves by sweeping the external in-plane field with a step size of 0.7 mT at fixed frequencies becomes an efficient way to characterize the local material properties. In Fig. 4(a) the resonance peaks are shown for different applied frequencies to the antenna at a nominal power of 20 dBm. The resonance peaks are fitted using Lorentz functions in order to get the resonance fields. These values are plotted in the inset together with the used frequencies and fitted by the Kittel formula [21]. The extracted values for the effective magnetization are $M_{\text{eff}} = 160 \text{ kA/m}$ and for the gyromagnetic ratio $\gamma/2\pi = 28.6$ GHz/T. Additionally, we show in Fig. 4(b) a direct comparison of the BLS intensity with and without antenna excitation of the sample at 3.2 GHz [compare to Fig. 4(a)]. The dashed and dash-dotted lines indicate the borders of the spin-wave band [20]. The highest spin-wave intensity can be excited around the FMR frequency. The inset shows the enlarged area of the excitation in order to show the large difference between the measured spin-wave intensity with and without the antenna excitation. No signal can be obtained if the antenna does not excite the YIG thin film. This strongly confirms the utility of our technique, since it opens up the possibility of investigating materials, which otherwise can not be measured with spatial resolution in a reasonable time by thermal excitation only.

As an additional example, we show the ferromagnetic resonance curves measured on a 240-nm-thick $Co_{40}Fe_{40}B_{20}$ sample. Figure 5(a) shows resonance curves for three different applied frequencies at a nominal power of 20 dBm and a distance of 15 μ m between the antenna and sample. The resonance curve obtained for the 11-GHz excitation is discussed in more detail in the following part. It is characterized by two resonances at different in-plane field values of 73.6 and 86.3 mT. We explain this behavior by calculation of the spin-wave dispersion relation [20] using $A_{\rm ex}=46$ pJ/m, $\mu_0 M_S=1.7$ T and the given

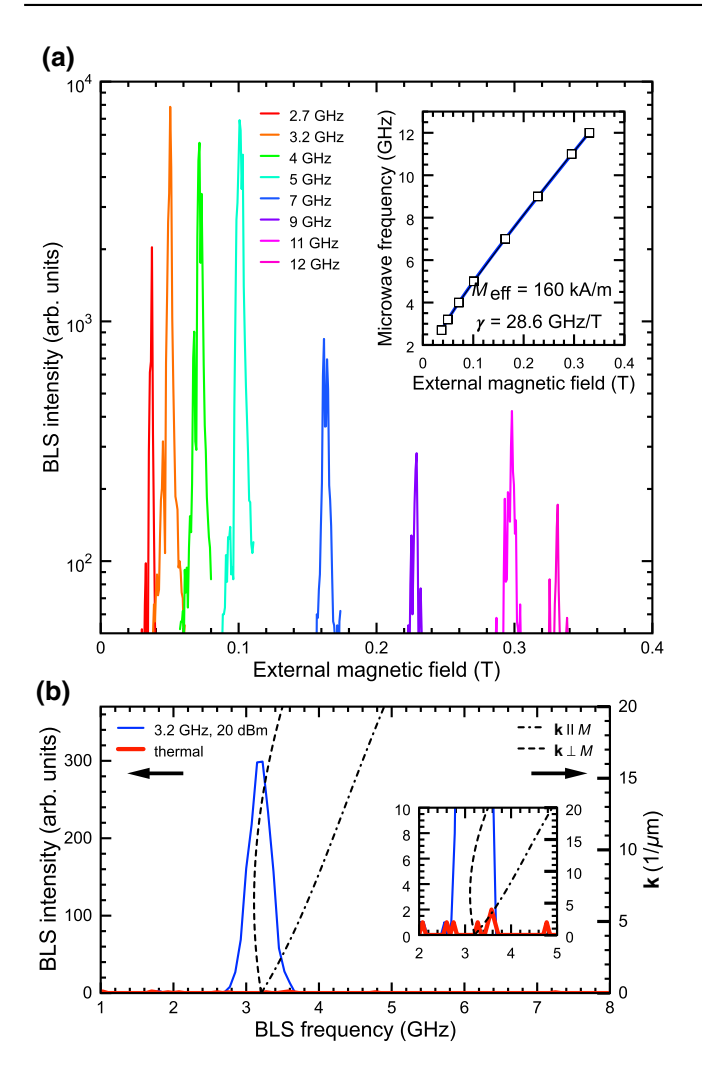


FIG. 4. (a) Ferromagnetic resonance peaks of a 50-nm YIG film measured by BLS during field sweeps with a step size of 0.7 mT using fixed microwave frequencies of the antenna. The inset shows the extracted resonance fields and corresponding excitation frequencies. Data is fitted by the Kittel formula in order to obtain $M_{\rm eff} = 160$ kA/m and $\gamma/2\pi = 28.6$ GHz/T. (b) Direct comparison of the BLS intensity with and without antenna excitation. The dashed and dashed-dotted lines indicate the borders of the spin-wave band calculated with these parameters: $M_S = 160$ kA/m, $\gamma/2\pi = 28.6$ GHz/T and $A_{\rm ex} = 5$ pJ/m. The inset shows the enlarged area at the excitation frequency. No signal could be obtained without antenna excitation.

external fields at the resonance. The mode number n specifies the shown spin-wave bands. A higher number n means in this case higher-energy modes across the film thickness also known as perpendicular standing spin waves (PSSW). Therefore, for fixed external magnetic fields, spin-wave bands with larger n are expected to range to higher frequencies. However, the frequencies of a certain band can be reduced by lowering the external magnetic field. As a consequence, spin-wave bands with higher number n can be excited at a constant excitation frequency by lowering

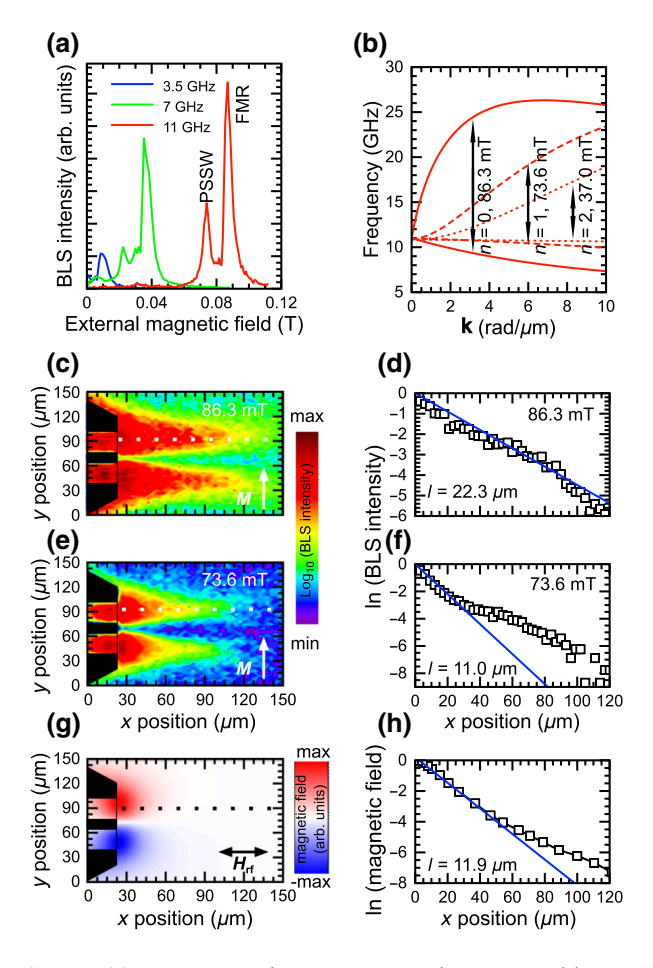


FIG. 5. (a) Ferromagnetic resonance peaks measured by BLS during field sweeps at fixed microwave frequencies of the antenna. (b) Spin-wave dispersion relation calculated for a 240-nm $\text{Co}_{40}\text{Fe}_{40}\text{B}_{20}$ film and $\mu_0M_S=1.7$ T, $A_{\text{ex}}=46$ pJ/m for different external fields and quantizations n across the film thickness. The continuous red (red-dashed) curves show the dispersion relation of the first n=0 (second, n=1) order of quantization across the film thickness. (c),(e) Spatially resolved measurements of the spin-wave intensity around the antenna (drawn in black) at external fields of 86.3 and 73.6 mT, respectively. (d),(f) Extracted BLS intensity along the white dotted lines in (c),(d) for the determination of the decay length for external magnetic fields of 86.3 and 73.6 mT, respectively. (g) Calculated magnetic in-plane field distribution around the antenna. (h) Exctracted field distribution along the black dotted line in (g).

the external magnetic field. It is found that the mode at the higher field can be attributed to spin waves close to k=0 for the n=0 spin-wave band. On the other hand, the resonance at the lower field can be attributed to spin waves close to k=0 for the n=1 spin-wave band [compare to Fig. 5(b)]. It shows, that the next quantization order n=1 of the spin waves across the film thickness is located at 11 GHz for $\mu_0 H_{\rm ext} = 73.6$ mT. Therefore, two resonances at similar magnetic fields are expected, if the excitation frequency is kept constant as in this experiment.

We also calculate the spin-wave band for the n = 2 quantization (red dotted lines) across the film thickness and find an expected resonance at 11 GHz for $\mu_0 H_{\text{ext}} = 37.0 \text{ mT}$. This can be an indication that the little increase of intensity at $\mu_0 H_{\text{ext}} = 37.0 \text{ mT}$ in the measurement shown in Fig. 5(a) is the excitation of spin waves with this particular quantization. For the n = 0 and n = 1 mode we did spatially resolve BLS measurements to have a deeper insight into the excitation profile of the antenna on the film. Figures 5(c) and 5(e) show the results for 86.3 and 73.6 mT, respectively. The position of the antenna is plotted in black. It is clearly visible, that both short circuits of the coplanar wave guide excite the magnetization equally indicating that the same amount of current is flowing through both of them. Starting from the short circuits, two narrow strong-excitation regions are detected. Between them the intensity drops significantly. This can be attributed to the 180° phase shift between both excitations. While the excited area for the measurement at 86.3 mT seems to be strongly extended to regions further away from the antenna, the one at 73.6 mT seems to be located closer to the antenna. To investigate this further, we extract the BLS intensity along the white dotted lines and plotted ln(BLS intensity) in Figs. 5(d) and 5(f), respectively. An exponential fit for the measurement at the higher field shows a close to linear behavior and allows for the determination of a decay length of 22.3 μ m for the BLS intensity, indicating a propagating spin-wave mode. For the smaller field, the extraction shows a deviation from a clear linear behavior, indicating a localized, directly excited mode in the close vicinity of the antenna. We fit only the points close to the antenna in order to obtain a decay length for comparison. A value of 11.0 μ m is obtained. From the fits it can be confirmed, that the excited mode at 86.3 mT extends further. The different propagation range of both modes can be explained by the spin-wave dispersion relation. The n=0mode includes much larger slopes, i.e., group velocities. Therefore, an extended propagation of these spin waves is expected compared to the spin waves with n = 1, which have smaller slopes. Since the area of excitation seems to be quite large even for $\mu_0 H_{\rm ext} = 73.6$ mT, we simulate the magnetic field distribution around the antenna with COM-SOL for the given antenna distance to the sample and plot the in-plane component in Fig. 5(g). Since the microwave wavelength is much larger than the short circuit generating the Oersted field, a static simulation is chosen using a constant dc current. It can be clearly seen, that the magnetic field generated on both sides has a phase difference of 180° generating a point of zero magnetic field in between. Similar to the measurements we extract the field distribution along the dotted line and plot it in Fig. 5(h). It is in qualitative agreement with Fig. 5(f), showing no linear behavior in the logarithmically scaled plot. The fit of values close to the antenna reveals a decay length of about 11.9 μ m, which is in good agreement with the value obtained from Fig. 5(f). Therefore, we conclude that the n = 1 mode at $\mu_0 H_{\text{ext}} = 73.6$ mT is a direct excitation in the close vicinity of the antenna rather than a propagating spin wave.

IV. INJECTION-LOCKING OF SPIN HALL NANO-OSCILLATORS

In this section we demonstrate the possibility of using the antenna device to perform injection-locking experiments with spin Hall nano-oscillators(SHNO). While in recent publications [22-24] microwave currents are directly applied to the SHNO to create a torque on the magnetization, we demonstrate here the synchronization of the magnetic auto-oscillations to the dynamic Oersted field of the suspended antenna device. The used SHNO [Fig. 6(a)] is fabricated using EBL and magnetron sputtering. The layer stack consists of $Ta(2 \text{ nm})/Pt(7 \text{ nm})/Co_{40}Fe_{40}B_{20}(5 \text{ nm})/Ta(2 \text{ nm})$. The Au contacts are deposited by thermal evaporation. Ta is used as the seed and capping layer. The applied dc current is mostly flowing through the Pt and generates a pure spin current via the spin Hall effect [25–27]. This pure spin current enters through the interface into the magnetic Co₄₀Fe₄₀B₂₀ layer. The magnetization of this layer is aligned perpendicular to the dc current by an external magnetic field, which is a necessary condition to obtain auto-oscillations of the magnetization [28–36]. Since magnetization and dc current are exactly perpendicular, we work at the point of maximized spin transfer torque. The auto-oscillations are localized in the 630-nmwide constriction, where the highest current density is reached [37]. Figure 6(b) shows the intensity of the autooscillations measured by BLS in dependence of the applied current at an external magnetic field of 34.5 mT. The autooscillations occur only in one current direction, whereas in the opposite current direction an increased damping of the magnetization is enforced. Please note also the negative nonlinear frequency shift of the auto-oscillations during the increase of current and the onset of the autooscillations, which is a typical property for SHNO with in-plane magnetization [30]. The increase of intensity and the negative nonlinear frequency shift correlate with each other. After the demonstration of auto-oscillations in the SHNO, the antenna is positioned close to the constriction and connected to a signal generator. The microwave frequency through the antenna is swept between 3.5 and 5 GHz in 25-MHz steps at a nominal power of 16 dBm and a dynamic Oersted field is generated affecting the magnetic layer of the SHNO. A dc current of 3.5 mA is applied to the SHNO at an external magnetic field of 34.5 mT. In Fig. 6(c) it is demonstrated that the auto-oscillations can synchronize to the dynamic Oersted field in a certain locking range. We separate the locking process into five segments [22]. If the difference between the frequency of the external stimulus and the auto-oscillations is too large

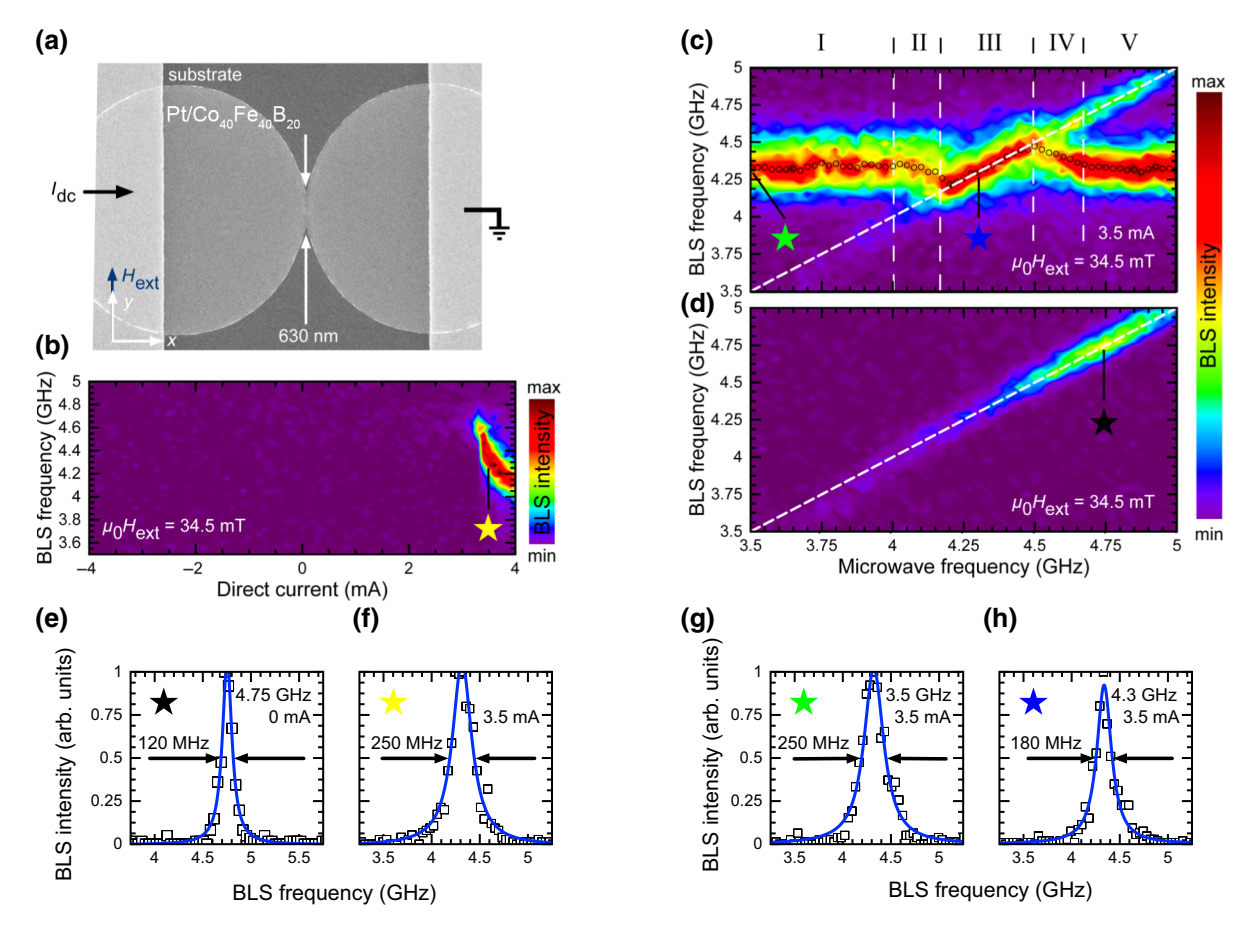


FIG. 6. (a) SEM image of the SHNO with a 630-nm-wide constriction. The external magnetic field $\mu_0 H_{\rm ext}$ is applied perpendicular to the dc current. (b) BLS intensity detected between 3.5 and 5 GHz as a function of the dc current ranging from -4.0 to +4.0 mA. A magnetic field of $\mu_0 H_{\rm ext} = 34.5$ mT is applied. For currents above 3.2 mA, a rapid increase in the intensity is observed, marking the threshold for the excitation of auto-oscillations. (c) Locking characteristics of the SHNO in Fig. 6(a) measured as a function of microwave frequency for a fixed $I_{\rm dc} = 3.5$ mA and $\mu_0 H_{\rm ext} = 34.5$ mT. The detected intensity is color-coded with violet (red) representing minimum (maximum) values. Black dots mark the frequencies $f_{\rm ao}$ of the excited auto-oscillations. Five different operating regimes can be identified: I, V free-running state of the auto-oscillation; II, IV frequency down and up pulling, respectively; III, the locked state. (d) Reference measurement without an applied dc current through the SHNO. (e) Linewidth of the microwave excitation at 4.75 GHz and a nominal power of 16 dBm. (f) Linewidth of the auto-oscillations at a dc current of 3.5 mA. (g) Linewidth of the auto-oscillations outside the locking state at 3.5 mA and an external stimulus of the antenna at 3.5 GHz. (h) Linewidth of the auto-oscillations in the locked state at 3.5 mA and an external stimulus of 4.3 GHz.

then there is no synchronization possible and the auto-oscillation frequency stays constant (segments I and V). However, if the difference between microwave and auto-oscillation frequency is reduced a frequency pulling sets in. The auto-oscillation frequency is stepwise shifted to the frequency of the external stimulus (segments II and IV). Within segment III the auto-oscillations are synchronized to the dynamic antenna field. This is indicated by the linear correlation between the external driven microwave frequency through the antenna and the auto-oscillation frequency in this segment. The included circles are obtained by fitting the measured spectra by Lorentz functions. Figure 6(d) shows the excitation from the antenna without auto-oscillations meaning that the dc current is switched off during this measurement. It can be clearly seen that

the direct spin-wave excitation within the locking range is much weaker than the auto-oscillation intensity. Please note that both plots are normalized to each other. Moreover, it can be seen from Fig. 6(d) that the intensity maximum is reached around 4.75 GHz marking the FMR. From this it can be concluded that the auto-oscillations are located at lower frequencies compared to the FMR. This is a well-known property of SHNO with in-plane magnetization and fits to the behavior of Fig. 6(b), where a red shift is detected. Figures 6(e)–6(h) compare the properties of the excited spin-wave modes within the SHNO. Figure 6(e) shows an extracted BLS spectrum with an antenna excitation at 4.75 GHz and without dc current. We fit it with a Lorentzian peak and obtain a linewidth value of 120 MHz, which can be treated as the linewidth

broadening of the BLS setup itself. Figure 6(f) shows in comparison a BLS spectrum, where only a dc current of 3.5 mA is present with no microwave current applied to the antenna. It can clearly be seen that the coherence of the auto-oscillations is much smaller, since the linewidth increases to 250 MHz. We directly compare this value with the linewidth of the auto-oscillations, where the additional stimulus by the antenna is applied. In Fig. 6(g) we plot the linewidth of the auto-oscillations at a dc current of 3.5 mA and an applied microwave frequency of 3.5 GHz at a nominal power of 16 dBm through the antenna. Since the applied microwave frequency is very different from the auto-oscillation frequency (about 4.3 GHz), no interaction is detected. This is confirmed by the same linewidth of the auto-oscillations of about 250 MHz. However, the linewidth significantly changes if a microwave frequency of about 4.3 GHz is applied to the antenna at the same nominal power. Figure 6(h) shows the reduction of the linewidth to 180 MHz in the locked state. It can be clearly seen that the injection locking of the auto-oscillations results in an increased coherence. Our method has several advantages with respect to the experimental schemes, which are used in previous publications. First, the microwave current is not applied directly to the SHNO, which eliminates additional heating. Second, for an efficiently generated torque via the microwave field the magnetization does not need to be tilted out of the geometry with the highest spin-torque efficiency. This means that the angle between magnetization and dc current can stay at 90°. Moreover, this is the geometry where the microwave field of our antenna transfers the largest torque on the magnetization. Injection locking in this geometry is only demonstrated before in a parametric pumping scheme to twice the auto-oscillator frequency [32]. The necessity of larger locking frequencies can be overcome by using the decoupled antenna. As demonstrated here, the locking can be achieved close to frequencies similar to the auto-oscillation frequency. This can be done otherwise by patterning an antenna directly on top of the structure only with significant effort, since additional insulation layers and contacts need to be patterned and deposited. In contrast to this approach a free-standing antenna allows the generation of an almost homogeneuos alternating field over several square micrometers.

V. CONCLUSION

We demonstrate the potential of a suspended antenna by comparing the obtained signal of thermal spin-wave measurements with the 400 times larger signal by additional external excitation. We show how thin films can be investigated with high spatial resolution by performing optical FMR measurements. Due to the additional excitation, the measurements on samples with very low signal, such as YIG thin films become not only possible, but

also highly efficient. Therefore, the magnetic properties, which can be accessed by spin waves like saturation magnetization, gyromagnetic ratio, damping, anisotropies, or even thickness, can be measured now with optical resolution. This can be done also in the presence of spin textures. We show the excitation of propagating spin waves in 240-nm-thick Co₄₀Fe₄₀B₂₀ films and explain the excitation characteristics by comparison to a simulation of the antenna field. Moreover, we are able to synchronize spin Hall nano-oscillators to the dynamic Oersted field generated by the antenna. During this process we are able to drive the auto-oscillations in the geometry of highest spin-transfer-torque efficiency meaning that the magnetization and the applied dc current are perpendicular to each other. Whereas locking in this special geometry can be done efficiently only in a parametric fashion to twice the auto-oscillation frequency, we are able to demonstrate it at frequencies in the range of the auto-oscillation frequency. By using the free-standing antenna we circumvent the additional heating of the spin Hall nano-oscillator by an applied microwave current. Since the antenna's microwave field points perpendicular to the magnetization within the SHNO the torque is also transferred in the most efficient geometry. Therefore, an efficient locking can be established although the antenna has no direct contact like an antenna directly patterned on the sample. Recently, one-dimensional and two-dimensional mutually synchronized SHNO arrays were demonstrated [38,39]. Despite the synchronization, the relative phase between the single oscillators deviates from zero, which reduces the output power. We believe that our method can mediate locking of one- and two-dimensional, mutual synchronized arrays in an efficient way. Thus, the phase differences of the single oscillators can be canceled to maximize the output power of these devices. We believe that our method can cause synergies to other magneto-optical methods like pump-probe experiments with short laser pulses. The interaction between spin waves excited by the antenna and laser pulses can be studied [40]. Moreover, the magnon amplitude in magnetoplasmonic crystals can be enhanced to increase the interaction with surface plasmon polaritions [41]. Beyond the scope of this work the application of localized microwave fields is also interesting for the investigation of magnetic nanoparticles and the excitation in optically detected magnetic resonance experiments, e.g., of SiC vacancy centers [42]. Additionally, the antenna device can be used also in nonoptical experiments for excitation of the magnetization, whereby the detection is realized via a vector network analyzer.

ACKNOWLEDGMENTS

Financial support by the Deutsche Forschungsgemeinschaft is gratefully acknowledged within program SCHU2922/1-1. The antennas are fabricated at the

CEITEC Nano Research Infrastructure (ID LM2015041, MEYS CR, 2016-2019). We thank B. Scheumann for deposition of the Au films. Lithography is done at the Nanofabrication Facilities (NanoFaRo) at the Institute of Ion Beam Physics and Materials Research at HZDR. I.B. acknowledges support by the National Science Foundation under Grant No. ECCS-1810541.

- K. Vogt, F. Y. Fradin, J. E. Pearson, T. Sebastian, S. D. Bader, B. Hillebrands, A. Hoffmann, and H. Schultheiss, Realization of a spin-wave multiplexer, Nat. Commun. 5, 3727 (2014).
- [2] Joel Cramer, Felix Fuhrmann, Ulrike Ritzmann, Vanessa Gall, Tomohiko Niizeki, Rafael Ramos, Zhiyong Qiu, Dazhi Hou, Takashi Kikkawa, Jairo Sinova, Ulrich Nowak, Eiji Saitoh, and Mathias Kläui, Magnon detection using a ferroic collinear multilayer spin valve, Nat. Commun. 9, 1089 (2018).
- [3] Z. Q. Qiu and S. D. Bader, Surface magneto-optic Kerr effect, Rev. Sci. Instrum. 71, 1243 (2000).
- [4] Simon Foner, Versatile and sensitive vibrating-sample magnetometer, Rev. Sci. Instrum. 30, 548 (1959).
- [5] V. Vlaminck and M. Bailleul, Spin-wave transduction at the submicrometer scale: Experiment and modeling, Phys. Rev. B 81, 014425 (2010).
- [6] Haiming Yu, O. d'Allivy Kelly, V. Cros, R. Bernard, P. Bortolotti, A. Anane, F. Brandl, R. Huber, I. Stasinopoulos, and D. Grundler, Magnetic thin-film insulator with ultralow spin wave damping for coherent nanomagnonics, Sci. Rep. 4, 6848 (2015).
- [7] J. Lucassen, C. Schippers, L. Rutten, R. Duine, H. Swagten, B. Koopmans, and R. Lavrijsen, Optimizing propagating spin wave spectroscopy, Appl. Phys. Lett. 115, 012403 (2019).
- [8] T. Sebastian, K. Schultheiss, B. Obry, B. Hillebrands, and H. Schultheiss, Micro-focused Brillouin light scattering: Imaging spin waves at the nanoscale, Front. Phys. 3, 35 (2015).
- [9] S.-C. Lee, C. P. Vlahacos, B. J. Feenstra, A. Schwartz, D. E. Steinhauer, F. C. Wellstood, and S. M. Anlage, Magnetic permeability imaging of metals with a scanning near-field microwave microscope, Appl. Phys. Lett. 77, 4404 (2000).
- [10] D. I. Mircea and T. W. Clinton, Near-field microwave probe for local ferromagnetic resonance characterization, Appl. Phys. Lett. 90, 142504 (2007).
- [11] L. A. Valiente, A. D. Haigh, A. A. P. Gibson, G. Parkinson, G. Jacobs, P. J. Withers, and R. Cooper-Holmes, in *Proceedings of the 37th European Microwave Conference* (IEEE, Munich, 2007), p. 194.
- [12] T. Satoh, Y. Terui, R. Moriya, B. A. Ivanov, K. Ando, E. Saitoh, T. Shimura, and K. Kuroda, Directional control of spin-wave emission by spatially shaped light, Nat. Photonics 6, 662 (2012).
- [13] Y. Au, M. Dvornik, T. Davison, E. Ahmad, P. S. Keatley, A. Vansteenkiste, B. Van Waeyenberge, and V. V. Kruglyak, Direct Excitation of Propagating Spin Waves by Focused

- Ultrashort Optical Pulses, Phys. Rev. Lett. 110, 097201 (2013).
- [14] S. Iihama, Y. Sasaki, A. Sugihara, A. Kamimaki, Y. Ando, and S. Mizukami, Quantification of a propagating spin-wave packet created by an ultrashort laser pulse in a thin film of a magnetic metal, Phys. Rev. B 94, 020401(R) (2016).
- [15] A. Kamimaki, S. Iihama, Y. Sasaki, Y. Ando, and S. Mizukami, Reciprocal excitation of propagating spin waves by a laser pulse and their reciprocal mapping in magnetic metal films, Phys. Rev. B 96, 014438 (2017).
- [16] Lukáš Flajšman, Kai Wagner, Marek Vaňatka, Jonáš Gloss, Viola Křižáková, Michael Schmid, Helmut Schultheiss, and Michal Urbánek, Zero-field propagation of spin waves in waveguides prepared by focused ion beam direct writing, Phys. Rev. B 101, 014436 (2020).
- [17] H. K. Lee, I. Barsukov, A. G. Swartz, B. Kim, L. Yang, H. Y. Hwang, and I. N. Krivorotov, Magnetic anisotropy, damping, and interfacial spin transport in Pt/LSMO bilayers, AIP Adv. 6, 055212 (2016).
- [18] R. Meckenstock and I. Barsukov, Imaging of ferromagnetic-resonance excitations in permalloy nanostructures on Si using scanning near-field thermal microscopy, J. Appl. Phys. 99, 08C706 (2006).
- [19] I. Barsukov, Yu Fu, A. M. Gonçalves, M. Spasova, M. Farle, L. C. Sampaio, R. E. Arias, and I. N. Krivorotov, Field-dependent perpendicular magnetic anisotropy in CoFeB thin films, Appl. Phys. Lett. 105, 152403 (2014).
- [20] B. A. Kalinikos and A. N. Slavin, Theory of dipoleexchange spin wave spectrum for ferromagnetic films with mixed exchange boundary conditions, J. Phys. C: Solid State Phys. 19, 7013 (1986).
- [21] C. Kittel, On the theory of ferromagnetic resonance absorption, Phys. Rev. 73, 155 (1948).
- [22] T. Hache, T. Weinhold, K. Schultheiss, J. Stigloher, F. Vilsmeier, C. Back, S. S. P. K. Arekapudi, O. Hellwig, J. Fassbender, and H. Schultheiss, Combined frequency and time domain measurements on injection-locked, constriction-based spin Hall nano-oscillators, Appl. Phys. Lett. 114, 102403 (2019).
- [23] T. M. Spicer, P. S. Keatley, M. Dvornik, T. H. J. Loughran, A. A. Awad, P. Dürrenfeld, A. Houshang, M. Ranjbar, J. Åkerman, V. V. Kruglyak, and R. J. Hicken, Time resolved imaging of the non-linear bullet mode within an injectionlocked nano-contact spin Hall nano-oscillator, Appl. Phys. Lett. 113, 192405 (2018).
- [24] K. Wagner, A. Smith, T. Hache, J.-R. Chen, L. Yang, E. Montoya, K. Schultheiss, J. Lindner, J. Fassbender, I. Krivorotov, and H. Schultheiss, Injection locking of multiple auto-oscillation modes in a tapered nanowire spin Hall oscillator, Sci. Rep. 8, 16040 (2018).
- [25] J. E. Hirsch, Spin Hall Effect, Phys. Rev. Lett. 83, 1834 (1999).
- [26] K. Ando, S. Takahashi, K. Harii, K. Sasage, J. Ieda, S. Maekawa, and E. Saitoh, Electric Manipulation of Spin Relaxation Using the Spin Hall Effect, Phys. Rev. Lett. 101, 036601 (2008).
- [27] A. Hoffmann, Spin Hall effects in metals, IEEE Trans. Magn. 49, 5172 (2013).

- [28] J. C. Slonczewski, Current-driven excitation of magnetic multilayers, J. Magn. Magn. Mater. 159, L1 (1996).
- [29] L. Berger, Emission of spin waves by a magnetic multilayer traversed by a current, Phys. Rev. B **54**, 9353 (1996).
- [30] A. Slavin and V. Tiberkevich, Nonlinear auto-oscillator theory of microwave generation by spin-polarized current, IEEE Trans. Magn. 45, 1875 (2009).
- [31] V. E. Demidov, S. Urazhdin, A. Zholud, A. V. Sadovnikov, and S. O. Demokritov, Nanoconstriction-based spin-Hall nano-oscillator, Appl. Phys. Lett. 105, 172410 (2014).
- [32] V. E. Demidov, H. Ulrichs, S. V. Gurevich, S. O. Demokritov, V. S. Tiberkevich, A. N. Slavin, A. Zholud, and S. Urazhdin, Synchronization of spin Hall nano-oscillators to external microwave signals, Nat. Commun. 5, 3179 (2014).
- [33] V. E. Demidov, S. Urazhdin, H. Ulrichs, V. Tiberkevich, A. Slavin, D. Baither, G. Schmitz, and S. O. Demokritov, Magnetic nano-oscillator driven by pure spin current, Nat. Mater. 11, 1028 (2012).
- [34] L. Yang, R. Verba, V. Tiberkevich, T. Schneider, A. Smith, Z. Duan, B. Youngblood, K. Lenz, J. Lindner, A. N. Slavin, and I. N. Krivorotov, Reduction of phase noise in nanowire spin orbit torque oscillators, Sci. Rep. 5, 16942 (2015).
- [35] Z. Duan, A. Smith, L. Yang, B. Youngblood, J. Lindner, V. E. Demidov, S. O. Demokritov, and I. N. Krivorotov, Nanowire spin torque oscillator driven by spin orbit torques, Nat. Commun. 5, 5616 (2014).

- [36] S. I. Kiselev, J. C. Sankey, I. N. Krivorotov, N. C. Emley, R. J. Schoelkopf, R. A. Buhrman, and D. C. Ralph, Microwave oscillations of a nanomagnet driven by a spin-polarized current, Nature 425, 380 (2003).
- [37] M. Dvornik, A. A. Awad, and J. Åkerman, Origin of Magnetization Auto-Oscillations in Constriction-Based Spin Hall Nano-Oscillators, Phys. Rev. Appl. 9, 014017 (2018).
- [38] A. A. Awad, P. Dürrenfeld, A. Houshang, M. Dvornik, E. Iacocca, R. K. Dumas, and J. Akerman, Long-range mutual synchronization of spin Hall nano-oscillators, Nat. Phys. 13, 292 (2017).
- [39] M. Zahedinejad, A. A. Awad, S. Muralidhar, R. Khymyn, H. Fulara, H. Mazraati, M. Dvornik, and J. Åkerman, Two-dimensional mutually synchronized spin Hall nanooscillator arrays for neuromorphic computing, Nat. Nanotechnol. 15, 47 (2020).
- [40] J. Walowski and M. Münzenberg, Perspective: Ultrafast magnetism and THz spintronics, J. Appl. Phys. 120, 140901 (2016).
- [41] N. Maccaferri, I. Zubritskaya, I. Razdolski, I.-A. Chioar, V. Belotelov, V. Kapaklis, P. M. Oppeneer, and A. Dmitriev, Nanoscale magnetophotonics, J. Appl. Phys. 127, 080903 (2020).
- [42] H. Kraus, V. A. Soltamov, D. Riedel, S. Väth, F. Fuchs, A. Sperlich, P. G. Baranov, V. Dyakonov, and G. V. Astakhov, Room-temperature quantum microwave emitters based on spin defects in silicon carbide, Nat. Phys. 10, 157 (2014).